Reversible Porosity Changes in Photoresponsive Azobenzene-Containing Periodic Mesoporous Silicas

Mercedes Alvaro, Miriam Benitez, Debashis Das, Hermenegildo Garcia,* and Encarna Peris

Instituto de Tecnologia Quimica CSIC-UPV and Departamento de Quimica, Universidad Politecnica de Valencia, Av. de los Naranjos s/n, 46022 Valencia, Spain

Received April 20, 2005. Revised Manuscript Received July 28, 2005

Two differently substituted azobenzenes having terminal trimethoxysilyl groups attached to the para position of the phenyl rings by means of different linkers have been used in combination with tetraethyl orthosilicate to prepare two periodic mesoporous organosilicas. As the corresponding precursors in solution, these solids exhibit a photochemical trans-to-cis isomerization of the azo group upon irradiation at 358 nm. The cis-configured isomer reverts to the trans isomer either photochemically upon irradiation at 450 nm or thermally at room temperature within days. As a consequence of the dramatic changes in the molecular dimension of azobenzene upon trans/cis isomerization, the adsorption of gold nanoparticles (1−10 nm) into the mesoporous silica depends reversibly on the trans or cis configuration of the azo groups grafted on the walls, the adsorption capacity of the *trans*-configured azobenzene being larger.

Introduction

Periodic mesoporous materials have an inorganic rigid structure defining channels of strictly regular dimensions in the nanometric scale.[1−3] This porosity is open to the exterior, allowing the mass transfer from a solution to the interior of the particles. Most of the interest in mesoporous materials derives from their ability to adsorb and incorporate functional guests in their internal voids.

One potential application of continuous films of micro- and mesoporous materials is as size-selective membranes allowing or impeding the passage through them of particles and species depending on whether their dimensions are smaller or larger than the pores.[4−13] These membranes of nanometric pores can even serve to separate molecules depending on their size and polarity. A representative example to illustrate the economical impact of these membranes is the selective separation of ethanol from ethanol−water vapors that is ready to enter in commercial application on a multi-ton scale.

Further development of porous silica membranes would be *intelligent* membranes in which the permeability and pore diameter of the membrane could be varied at will by applying an external stimulus.[14−16] An example of these *intelligent* membranes would be photoactivable membranes whose pore size could be switched between two states based on to the photochemical interconversion between two isomers.[17,18]

Herein, we report a photoresponsive periodic mesoporous organosilica (PMO) whose adsorption ability varies reversibly in a controllable way upon irradiation. The PMOs contain azobenzene groups whose more stable trans isomer undergoes a photochemical trans/cis isomerization to form the cis isomer. We have found that the cis-configured azobenzene derivative is, however, not stable at room temperature under ambient conditions and undergoes a dark relaxation back to the more stable trans isomer with a lifetime of several days. The photochemical-thermal cycle is fairly reversible and no fatigue of the trans−cis interconversion has been observed after 10 cycles. This work is related to previous ones in which azobenzene has been used as photoresponsive chromophore in clays to alter the intergallery space or in mesoporous MCM-41 to control the access to

* To whom correspondence should be addressed. E-mail: hgarcia@quim.upv.es.

(1) Inagaki, S.; Guan, S.; Fukushima, Y.; Oshuna, T.; Terasaki, O. *J. Am. Chem. Soc.* **1999**, *121*, 9611−9614.
(2) Asefa, T.; MacLachlan, M. J.; Grondey, H.; Coombs, N.; Ozin, G. A. *Angew. Chem., Int. Ed.* **2000**, *39*, 1808−1811.
(3) MacLachlan, M. J.; Asefa, T.; Ozin, G. A. *Chem. Eur. J.* **2000**, *6*, 2507−2511.
(4) Jeong, H.-K.; Nair, S.; Vogt, T.; Dickinson, L. C.; Tsapatsis, M. *Nat. Mater.* **2003**, *2*, 53−58.
(5) Weh, K.; Noack, M.; Sieber, I.; Caro, J. *Microporous Mesoporous Mater.* **2002**, *54*, 27−36.
(6) Lassinantti, M.; Jareman, F.; Hedlund, J.; Creaser, D.; Sterte, J. *Catal. Today* **2001**, *67*, 109−119.
(7) Wan, Y. S. S.; Chau, J. L. H.; Gavriilidis, A.; Yeung, K. L. *Microporous Mesoporous Mater.* **2001**, *42*, 157−175.
(8) Hedlund, J.; Noack, M.; Kolsch, P.; Creaser, D.; Caro, J.; Sterte, J. *J. Membr. Sci.* **1999**, *159*, 263−273.
(9) Noack, M.; Koelsch, P.; Venzke, D.; Toussaint, P.; Caro, J. *Stud. Surf. Sci. Catal.* **1995**, *98*, 276−277.
(10) Koelsch, P.; Venzke, D.; Noack, M.; Toussaint, P.; Caro, J. *J. Chem. Soc., Chem. Commun.* **1994**, 2491−2492.
(11) Koelsch, P.; Venzke, D.; Noack, M.; Lieske, E.; Toussaint, P.; Caro, J. *Stud. Surf. Sci. Catal.* **1994**, *84*, 1075−1082.
(12) Noack, M.; Koelsch, P.; Venzke, D.; Toussaint, P.; Caro, J. *Microporous Mater.* **1994**, *3*, 201−206.
(13) Matsukata, M.; Nishiyama, N.; Ueyama, K. *J. Chem. Soc., Chem. Commun.* **1994**, 339−340.
(14) Ozin, G. A.; Kuperman, A.; Stein, A. *Angew. Chem.* **1989**, *101*, 373−390.
(15) Weh, K.; Noack, M. *Host−Guest−Syst. Nanoporous Cryst.* **2003**, 484−500.
(16) Kim, Y.; Dutta, P. K. *Res. Chem. Intermed.* **2004**, *30*, 147−161.
(17) Weh, K.; Noack, M.; Hoffmann, K.; Schroder, K. P.; Caro, J. *Microporous. Mesoporous. Mater.* **2002**, *54*, 15−26.
(18) Noack, M.; Kolsch, P.; Caro, J.; Weh, K. *Eur. Pat. Appl.* **2001**, 1095694.

10.1021/cm050837z CCC: $30.25
Published on Web 09/03/2005

Scheme 1

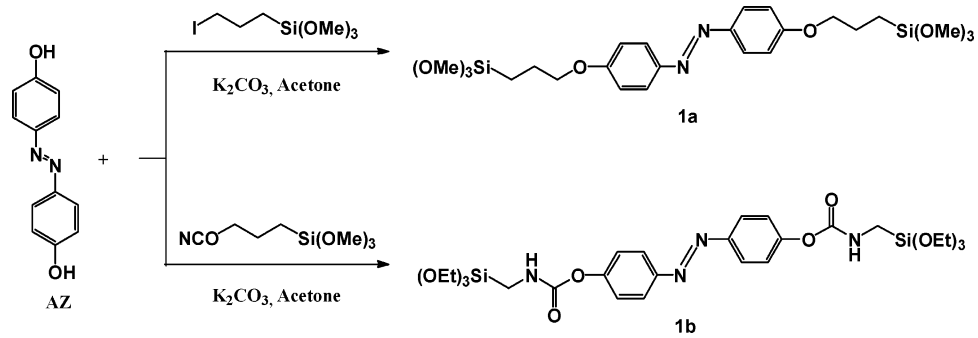

the pores.[19−25] Our material contains azobenzene groups uniformly distributed inside the pores and these azobenzene components control the channel tortuosity, pore size, and adsorption capacity of the porous material.

Results and Discussion

Cis/trans isomerization in azobenzenes is a very well-known photochemical reaction.[26] Upon excitation of the thermodynamically more stable trans isomer at its λ_{max} wavelength (typically around 350 nm), it undergoes a one-way isomerization to be a less stable cis isomer. The cis isomer has a different absorption spectrum, absorbing at longer wavelengths with lower extinction coefficient. The UV−Vis spectra of the trans and cis azobenzene are sufficiently different to allow almost selective excitation of any of the two stereoisomers. The less stable *cis*-azobenzene can undergo either a photochemical isomerization to the trans isomer upon irradiation at λ_{max} of this isomer (typically 450 nm), or alternatively the cis isomer can also isomerize thermally to the trans, although thermal isomerization at room temperature can be slow.

This well-known photochemical behavior constitutes the basis of the photochemical activity of two azobenzene-containing PMOs synthesized in this work. In our case we have prepared two different organosilica compounds that were obtained in a single step from 4,4′-dihydroxyazobenzene. Analytical and spectroscopic data confirmed the proposed chemical structures of compounds **1a** and **1b**. Scheme 1 shows the reagents and conditions under which the synthesis of the organosilane precursors were made.

The photochemical behavior of 4,4′-dihydroxyazobenzene and precursors **1a**,**b** was studied in acetonitrile solution, monitoring the course of the photochemical isomerization by transmission UV−Vis spectroscopy. Figure 1 shows two series of spectra recorded for precursors **1a** and **1b**. As expected, the initial UV−Vis spectrum of precursors **1a** and **1b** corresponded predominantly to the trans isomer, and upon irradiation at 355 nm, a decrease of the trans characteristic absorption band and the appearance of the expected absorption for the cis isomer (λ_{max} 440 and 435 nm for ***cis*-1a** and ***cis*-1b**, respectively) was observed. In agreement with the selective transformation trans-to-cis, clear isosbestic points at 425 and 405 nm were recorded for **1a** and **1b**, respectively. Importantly, upon standing at room temperature in the dark the absorption band of the cis isomers decay gradually with the concomitant growth of that corresponding to the trans isomers. This indicates that the photochemical trans-to-cis isomerization is reversed thermally in the dark. The thermal interconversion cis to trans in solution was complete in less than 24 h. This cycling, irradiation at 355 nm and thermal relaxation, was repeated in acetone 10 times without noticeable fatigue in the systems.

Once the behavior of precursors **1a** and **1b** was studied in solution, we proceeded to prepare PMO solids containing the azobenzene units. Photochemical trans/cis isomerization of azobenzenes adsorbed or included in silicates and inorganic oxides has been widely used in order to have photoresponsive materials that exhibit some photochemical reversibility.[15,17,19−22,24] Most of this reported work takes advantage of the remarkable changes in the molecular length when *trans*-azobenzene (∼0.9 nm length) is transformed into *cis*-azobenzene (∼0.5 nm length), this drastic variation being responsible for the effect observed in the material. In this regard, we have recently reported a PMO containing 1,2-bis-pyridylethylene units that upon photochemical isomerization reaches a photostationary state of cis and trans isomer that was thermally stable.[27] In that case, the photochemical isomerization was accompanied by persistent changes in pore diameter and internal surface area. In the case reported here, based on the reversibility of the azobenzene isomerization for derivatives **1a** and **1b**, we expected the system to be reversible, varying the pore size due to trans to cis isomerization upon irradiation and then the system relaxing to the initial pore size upon standing in the dark for sufficiently long time periods. Our expectances are based on the behavior of the organosilane precursors **1a** and **1b** in solution.

The resulting PMOs contain both photoactive azobenzene moieties covalently linked to the inorganic silica porous structure by propyl linkers (AZ-1∝PMO) or carbamate

(19) Ogawa, M.; Kuroda, K.; Mori, J.-i. *Chem. Commun.* **2000**, 2441−2442.
(20) Liu, N.; Chen, Z.; Dunphy, D. R.; Jiang, Y.-B.; Assink, R. A.; Brinker, C. J. *Angew. Chem., Int. Ed.* **2003**, *42*, 1731−1734.
(21) Kawashima, Y.; Nakagawa, M.; Seki, T.; Ichimura, K. *Trans. Mater. Res. Soc. Jpn.* **2002**, *27*, 509−512.
(22) Ogawa, M.; Goto, R.; Kakegawa, N. *Clay Sci.* **2000**, *11*, 231−241.
(23) Hoffmann, K.; Prescher, D.; Marlow, F. *J. Inform. Record.* **1998**, *24*, 191−196.
(24) Anzai, J.-i.; Osa, T. *Tetrahedron* **1994**, *50*, 4039−4070.
(25) Kumar, G. S.; Neckers, D. C. *Chem. Rev.* **1989**, *89*, 1915−1925.
(26) Gilbert, A.; Baggott, J. *Essentials of Organic Photochemisry*; Blackwell: Oxford, 1990.
(27) Alvaro, M.; Ferrer, B.; Garcia, H.; Rey, F. *Chem. Commun.* **2002**, 2012−2013.

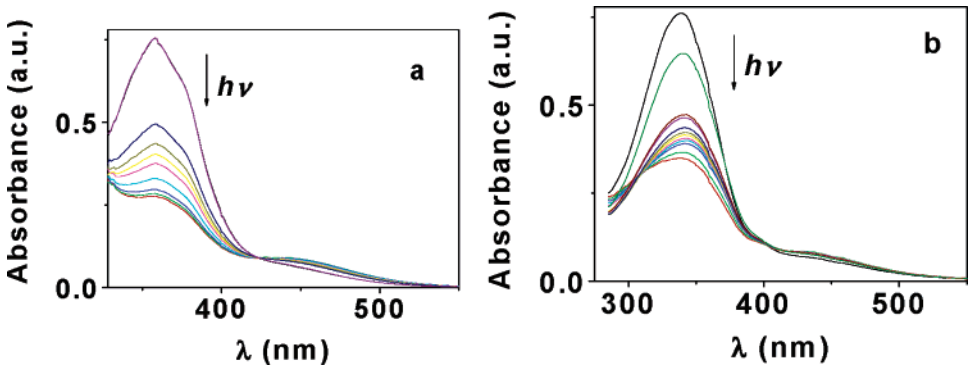

Figure 1. Transmission UV−Vis spectra of precursors **1a** (a) and **1b** (b) upon irradiation at 355 nm in acetonitrile. The peaks at about 350 nm are characteristic of the trans isomer, while the peaks at about 430 nm correspond to the cis isomer.

Scheme 2

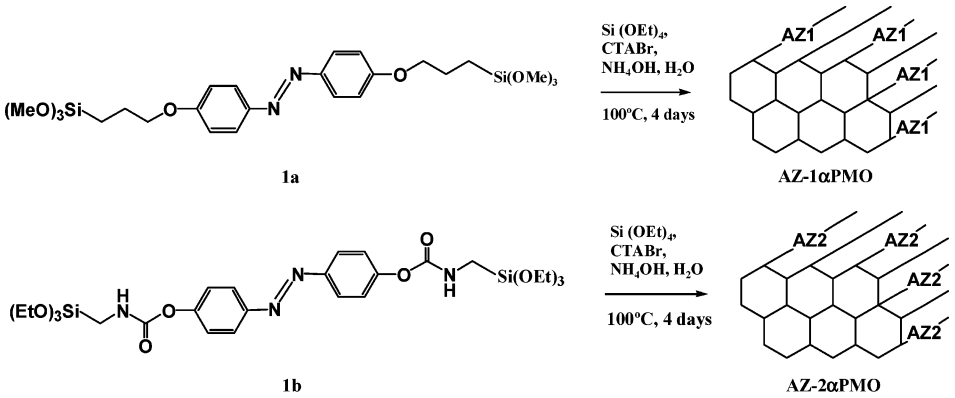

groups (AZ-2∝PMO). Preparation was carried out as indicated in Scheme 2 under typical synthetic conditions for PMOs using cetyltrimethylammonium (CTA^+) as the structure directing agent and basic conditions.

The typical molar composition of the gels used in the synthesis of the PMOs was as follows: 1.00:0.12:8.0:114 Si:CTABr:NH_3 (20%):H_2O. As the silicon atom source we used a mixture of TEOS and precursors **1a** or **1b** in a 95:5 molar ratio, corresponding to TEOS:silylated organic product ratio in weight of 87.5:12.5. After crystallization, the solids were submitted to solid liquid extraction to remove the CTABr surfactant as well as residual organosilanes not covalently bonded to the PMO walls. The crystallinity of the AZ-1∝PMO and AZ-2∝PMO before and after extraction was checked by powder XRD.

Figure 2 shows the XRD patterns of as-synthesized and extracted PMO in where the characteristic peak at $2\theta = 2°$ and the associated d_{110} and d_{200} peaks corresponding to a MCM-41 like structure can be seen. As expected in view of the general behavior of related materials, the crystallinity of AZ-1∝PMO is reduced after removal of the template. However, it is important to note that AZ-1∝PMO has still periodic structure after removal of the template as indicated by the presence of the 2° peak powder XRD and by isothermal gas adsorption (see Figure 3). The case of the carbamate-containing AZ-2∝PMO is remarkable since the number of counts in powder XRD even increased upon removal of the template. This unexpected fact is most probably related to the presence of strong hydrogen bond interactions in the carbamate units. It has been reported that related urea motifs can serve to template the mesoporous solids even in the absence of a structure directing agent.[28] Isothermal nitrogen adsorptions show the typical profile corresponding to mesoporous materials, whereby a BET surface area of 492 and 540 $m^2\ g^{-1}$ with mononodal pore size distribution around 2.6 and 3.0 nm were estimated for AZ-1∝PMO and AZ-2∝PMO, respectively.

The actual content of azobenzene units in the PMO solids was determined by combustion C and N chemical analysis of surfactant-free PMOs giving value of 0.01 mmol g^{-1} for AZ-1∝PMO and AZ-2∝PMO. According to these analytical data, the PMOs contained about 70% of the maximum possible azobenzene loading based on the gel composition (about 8 wt % of organic material). The presence of the azobenzene chromophores can be clearly observed in the diffuse reflectance UV/Vis of the solids that closely agree with the spectra of the precursors in solution. Also, IR spectroscopy shows the presence of azobenzene units in the PMO characterized by the aromatic stretching vibration in the 1600−1400 cm^{-1} zone of the IR spectra (Figure 4).

As expected, in view of the photochemical behavior of precursors **1a** and **1b** in solution, the photochemical irradiation of the PMO powders leads to changes in the optical spectrum of the solids that are compatible with the occurrence of the photochemical trans-to-cis isomerization of the azo group. Figure 5 illustrates the variations that are observed in the optical spectra of the solids, recorded by diffuse reflectance mode. Upon standing in the dark for 24 h, the initial optical spectrum was restored.

(28) Moreau, J. J. E.; Pichon, B. P.; Man, M. W. C.; Bied, C.; Pritzkow, H.; Bantignies, J.-L.; Dieudonne, P.; Sauvajol, J.-L. *Angew. Chem., Int. Ed.* **2003**, *43*, 203−206.

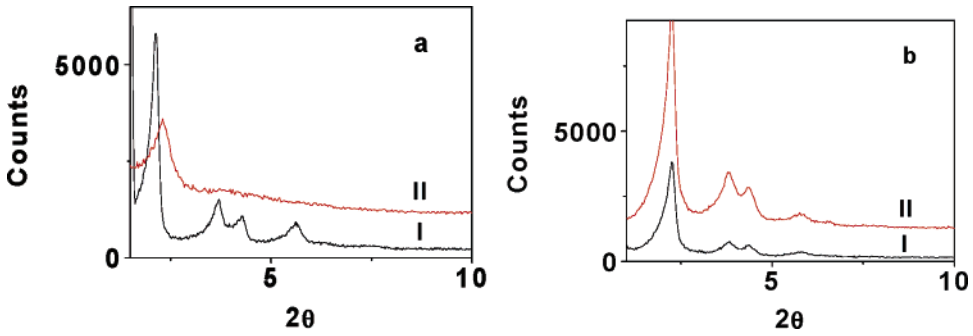

Figure 2. Powder XRD of AZ-1∝PMO (a) and AZ-2∝PMO (b) before (I) and after (II) removal of CTABr.

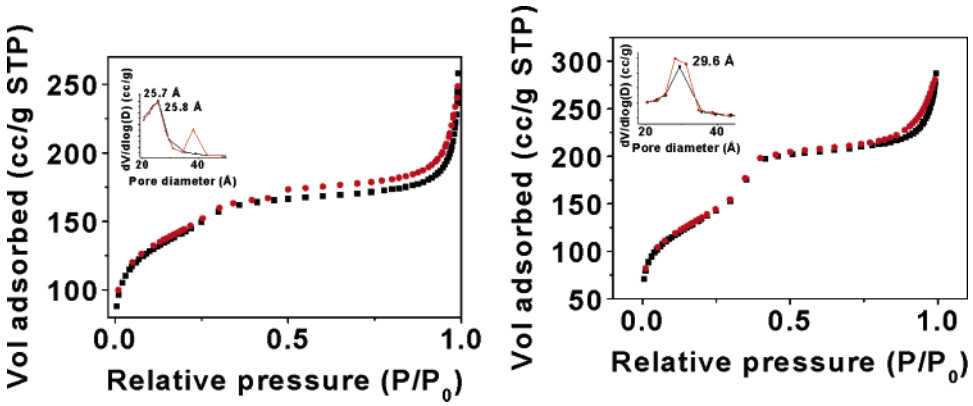

Figure 3. Isothermal N_2 gas adsorption−desorption of AZ-1∝PMO (left) and AZ-2∝PMO (right) from which the data of BET surface area and pore size distribution have been obtained. The inset shows the pore size distribution based on the adsorption or desorption branch of the isotherm.

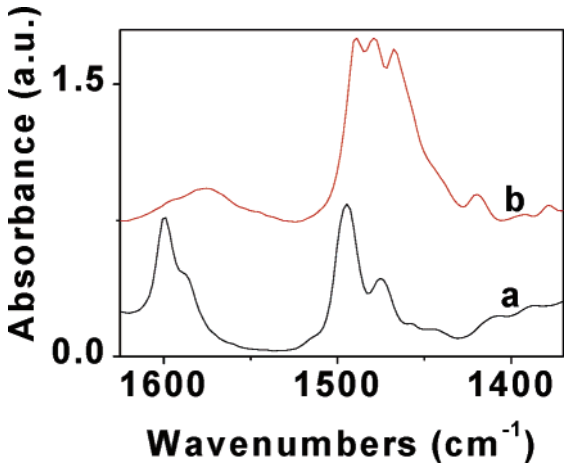

Figure 4. Aromatic region of the IR spectra of AZ-1∝PMO (plot a) and AZ-2∝PMO (plot b) recorded in a sealed cell after removal of CTA^+. The sample was previously evacuated at 100 °C under 10^{-2} Pa before recording the IR spectra at room temperature.

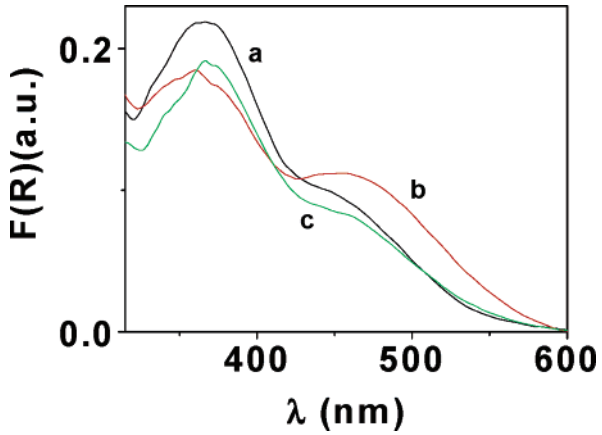

Figure 5. Optical spectra recorded for AZ-1∝PMO by diffuse reflectance mode before (a), immediately after 355 nm irradiation of the surface for 5 min (b), and after an elapsing time of 24 h after irradiation (c).

This cycling consisting of the photochemical trans-to-cis isomerization and subsequent thermal cis-to-trans relaxation was repeated five times without significant differences between them. With use of highly structured samples before removal of CTAB template, XRDs immediately after irradiating for several hours showed clearly a small but significant shift in the position of the peaks, indicating that the photoisomerization has resulted in a variation of the structure. The changes undergone by the XRD upon irradiation were reproducible and out of the error of the measurements. Figure 6 shows the changes for AZ-1∝PMO before and after irradiation that according to the Bragg law correspond to a reduction of the *d* spacing from 41.25 to 40.40 nm. This change would be compatible with the occurrence of a reduction of pore size.

The thermal instability of the cis-configured azobenzene isomers precludes direct measurement of the porosity changes and pore size distribution variations after irradiation since the technique of isothermal gas adsorption requires a thermal pretreatment to desorb water before the measurements. However, we have been able to demonstrate the occurrence of these changes in the porosity arising from the photochemical trans-to-cis isomerization by observing differences in the adsorption ability of the azobenzene-containing PMOs before and after irradiation.

Considering the diameter of the AZ-1∝PMO and AZ-2∝PMO in the nanometer scale, we anticipated that the photochemical trans-to-cis isomerization should provoke a

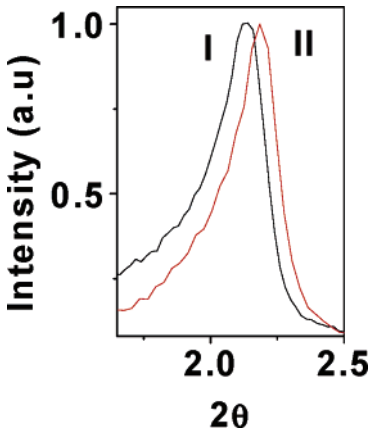

Figure 6. Powder XRD of AZ-1∝PMO before (I) and immediately after (II) 3 h irradiation.

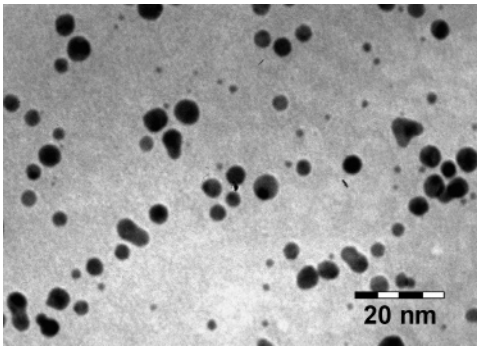

Figure 7. TEM image of the colloidal gold nanoparticles used in the adsorption experiments. Only those particles whose diameter is smaller than the mesopore opening of the PMOs (about 3 nm) can be adsorbed inside the voids.

reduction of pore size in the nanometer scale since the trans-configured azobenzene has a smaller kinetic diameter than the cis-configured isomer. Therefore, this photochemical reaction could be reflected in differences in the adsorption capacity for guests of nanometer dimensions. To demonstrate this photoresponsive porosity change, we prepared colloidal gold sols following reported procedures.[29] The advantages of using colloidal gold nanoparticles derive from the reproducibility in the preparation of these colloids, their nanometric size, the strong coloration of the colloid that allows easy monitoring of the adsorption, and the growing interest in supported gold nanoparticles as solid catalysts. Reliable preparation procedures starting from $AuCl_4^-$ are known to give colloidal gold nanoparticles in the 1−20 nm range.[29] Actually, a representative TEM image of the colloidal gold sol used in the adsorption experiments is shown in Figure 7. Statistical analysis of a set of 500 × 500 nm^2 images shows a distribution of particle size in the range 1−20 nm. Importantly, a significant population of these gold particles can be included inside the pores of AZ-1∝PMO (2.6 nm) and AZ-2∝PMO(3.0 nm), although some others have a diameter larger than 4 nm and cannot be adsorbed in these mesoporous solids. As expected in view of their somewhat different pore size distribution, absorption of gold nanoparticles on AZ-1∝PMO was somewhat less than in AZ-2∝PMO (see Table 1). Thus, in an ideal adsorption experiment, the supernatant should be depleted of smaller particles and only larger particles would remain.

(29) Daniel, M.-C.; Astruc, D. *Chem. Rev.* **2004**, *104*, 293−346.

Table 1. Percentage of Colloidal Gold Present in Solution (4 mL of a 1.032 × 10^{-4} mg mL^{-1}) That Becomes Adsorbed on the Solid (67 mg) upon Magnetic Stirring at Room Temperature for 1 h Depending on the Treatment To Which the Solid Was Submitted

sample	unirradiated	irradiated upon storage for 8 h in the dark	immediately after irradiation
AZ-1∝PMO	83	73	64
AZ-2∝PMO	88	81	74

The relatively broad particle size distribution, with the colloid having some particles that can access the interior of the mesoporous solids and some others that cannot access, is useful to rule out preferential adsorption on the external surface as being responsible for the decrease of gold nanoparticles in the colloid. Thus, it is expected that the colloid will change the particle size distribution upon adsorption due to the preferential adsorption of smaller gold nanoparticles inside the mesopores. To confirm this, we performed some experiments using conditions analogous to those in Table 1 but using larger excess of AZ-2∝PMO solid (120 mg). Based on TEM images, we compared the particle size distribution of the gold nanoparticles in the liquid phase before and after adsorption. The results are shown in Figure 8. As can be seen there, adsorption leads to a remarkable change in the particle size, the colloid present in the liquid phase having a significant higher percentage of larger particles, as expected.

As commented before, one advantage of using colloidal gold sols for these adsorption studies is that the course of the adsorption can be simply followed by monitoring in UV/Vis spectroscopy the intensity of the plasmon adsorption band characteristic of colloidal gold nanoparticles at λ_{max} 530 nm in the supernatant solution. As expected, upon contact of the purple gold dispersion in water with the PMOs, the pink color fades gradually in the solution while the solid becomes concomitantly colored. The intensity of the plasmon visible band of the colloidal suspension can be used to quantify the amount of gold remaining in the liquid phase and, therefore, by the difference in the amount of gold that has been adsorbed into the solid. As Figure 9 shows, we observed significant and reliable differences in the adsorption of colloidal gold nanoparticles both for AZ-1∝PMO and AZ-2∝PMO before and after irradiation of the powders to effect the trans−cis isomerization. We have also observed a minor blue shift in λ_{max} of about 10 nm for the gold nanoparticles remaining in the colloidal suspension with respect to the λ_{max} value before adsorption. This variation in λ_{max} would indicate a change in the particle size of the gold particles left in the colloidal solution toward large particles, indicating a preferent adsorption of smaller particle size gold particles.

The AZ-1∝PMO and AZ-2∝PMO materials stored in the dark adsorb a significantly higher amount of the colloidal nanoparticles than those after irradiation and conversion of azobenzene in the cis form. The actual data summarizing the adsorption capacity under our irradiation conditions are collected in Table 1.

Furthermore, upon standing in the dark at room temperature for 8 h, the irradiated solid recovers a large part of the

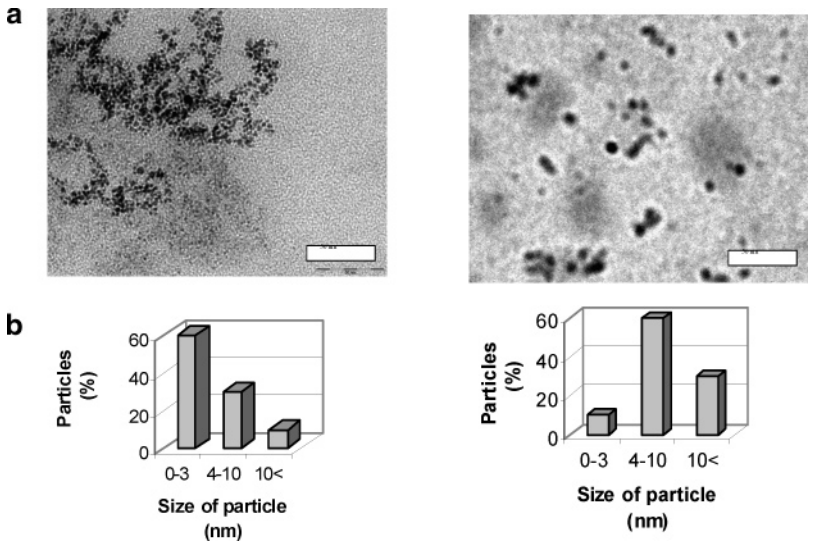

Figure 8. Top: TEM images of gold nanoparticles present in the liquid phase before (left) and after adsorption (right) on AZ2∝PMO. Bottom: Particle size distribution of the nanoparticles before (left) and after adsorption (right).

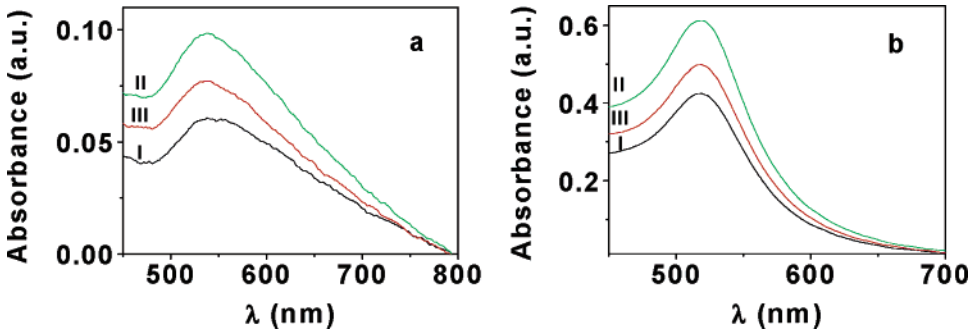

Figure 9. UV/Vis spectrum corresponding to the plasmon band of colloidal gold nanoparticles present in the solution (initial concentration about 10^{-4} mg mL^{-1}) when twin PMO samples are contacted without (I) or after 15 min of irradiation (II). Spectra (III) correspond to sample (II) that has been stored in the dark 8 h before contacting the solution under the same conditions as I and II. Plots a and b correspond to the AZ-1∝PMO and AZ-2∝PMO series, respectively.

initial adsorption capacity of the fresh sample. Longer storage times of the irradiated samples led to an almost complete recovery (over 97 %) of the adsorption capacity of the PMO solid. These experiments were repeated four times whereby exactly the same behavior was observed.

The variation in the adsorption capacity upon irradiation can be interpreted in a simple way based on the photochemical behavior of the azobenzene chromophore described earlier. Thus, according to the optical spectrum, the initial AZ∝PMOs contain mainly the trans-configured isomer and exhibited larger pore size, sufficiently large to adsorb a percentage of the gold nanoparticles depending on their particle size. Upon irradiation at 355 nm for a short time, a population of trans azobenzene undergoes isomerization to the cis form, reducing effectively the size of the mesopores in the region where this is reflected in the percentage of metal particle adsorption. Therefore, upon irradiation the number of gold nanoparticles that can be adsorbed decreases. The photochemical trans−cis isomerization is thermally reversible and upon storage the population of cis-azobenzene decay back to the trans isomer and the adsorption capacity is gradually (days) restored.

The photoinduced change in the adsorption capacity of azobenzene containing PMOs could be useful for the development of photoresponsive membranes. For this application, films of the material should be prepared on the surface of a porous support. To determine the feasibility of these films, we attempted the preparation of AZ-2∝PMO on a quartz slide by pouring the synthesis gel on the substrate and heating the system in an oven at 80 °C. XRD of the resulting solid showed, however, that a layered rather than a hexagonal phase was obtained. Further work in which the chamber humidity and temperature is optimized would be necessary to obtain a film with the hexagonal PMO phase.

In conclusion, here we provide evidence for a photoresponsive material synthesized following the PMO concept that exhibits reversible change in adsorption capacity derived from the changes in the molecular dimensions of azobenzene in the trans and cis configuration. The above finding can be useful in the development of photoresponsive films and membranes based on the PMO materials.

Experimental Section

Reagents and solvents were obtained from commercial sources and were used without further purification.

Synthesis of 4,4′-Bis(3-trimethoxysilylpropoxy)azobenzene (1a). 4,4-Dihydroxyazobenzene was prepared as previously reported.[30,31] To a solution of 4,4′-dihydroxyazobenzene (500 mg, 2.34 mmol) dissolved in 20 mL of dry acetone kept under an Ar atmosphere, K_2CO_3 (1.937 g, 14.02 mmol) and 3-iodopropyl-

trimethoxysilane (1.423 g, 4.91 mmol) were added under an Ar atmosphere and the suspension stirred magnetically at reflux temperature for 40 h. After this time, the suspension was filtered to remove the K_2CO_3, and the solvent was evaporated under reduced pressure to obtain an orange oil (682 mg, 1.27 mmol, 54%) that was used in the preparation of AZ-1∝PMO without further purification. Analytical and spectroscopic data of **1a**: HRMS for $C_{22}H_{34}N_2O_8Si_2$ 510.18537; found 482.15366. FT-IR wavenumber (cm^{-1}, CH_2Cl_2): 2958, 2923, 2854, 1598, 1494, 146, 1403, 1244. ^1H NMR δ (ppm, $CDCl_3$): 0.89 (4H, t, 7 Hz, SiCH_2), 1.65 (m, 4H, $CH_2CH_2CH_2$), 3.60 (s, 18 H, SiOCH_3), 3.84 (4H, t, 7 Hz, OCH_2), 6.64−7.38 (aromatics). ^{13}C NMR δ (ppm, $CDCl_3$).

Synthesis of the AZ-1∝PMO. Periodic mesoporous organosilica AZ-1∝PMO was obtained by mixing the reactants to get a uniform white gel. TEOS and silylated organic precursors **1a** were used as the silicon source and hexadecyltrimethylammonium bromide (CTABr) as the structure-directing agent. The typical molar composition of the gel was as follows: 1.00:0.12:8.0:114 Si:CTABr:NH_3 (20%):H_2O.

The experimental procedure was as follows: 0.325 g of CTABr was added to a solution of NH_4OH (7.444 g, 28 wt %) and deionized water (9.90 g) and the solution was stirred for 30 min in a closed polyethylene bottle to form a homogeneous solution. This solution was cooled at 10 °C. To this solution, Si from TEOS (1.17 g) and silylated organic product **1a** (0.500 g dissolved in 1 mL of water/acetone 3:1) was slowly added. After the reactants were mixed, the resulting gel was stirred for 1 h while the temperature gradually increased up to room temperature. Then, the solution was heated at 100 °C in static conditions for 4 days. The solid obtained was washed thoroughly with water and dried at 100 °C for 3 h. The structure-directing agent was removed by extracting the solid first with 0.05 M ethanolic HCl acid solution (10 mL per g of solid at 50 °C for 3 h) and then with 0.15 M HCl/EtOH:*n*-heptane (48:52) (25 mL per g of solid) 90 °C for 12 h. Chemical analysis of the extracted material gives 7.00% for C.

Synthesis of 4,4′-Bis(3-trimethoxysilylpropylaminocarbonyloxy)azobenzene (1b). 4,4′-Dihydroxyazobenzene (300 mg, 1.40 mmol) and 3-isocyanatepropyltriethoxysilane (0.692 μL, 2.80 mmol) were stirred magnetically under an Ar atmosphere at reflux temperature for 24 h. Compound **1b** was obtained as a red solid (526 mg, 0.77 mmol, 53%). FT-IR (cm^{-1}): 1650.

Synthesis of AZ-2∝PMO. AZ-2∝PMO was synthesized from TEOS and silylated organic precursor **1b** as silicon source and CTABr as the structure-directing agent. The typical molar composition of the gel was as follows: 1.00:0.12:8.0:114 Si:CTABr:NH_3 (20%):H_2O. The experimental procedure was as follows: CTABr (1.297 g, 355.8 mmol) was added to a solution of NH_4OH (29.695 g, 237.2 mmol, 28 wt %) and deionized water (39.467 g, 3.4 mol), and the solution was stirred for 30 min in a closed polyethylene bottle to form a homogeneous solution and cooled to 10 °C. To this solution, Si from TEOS (2.0 g, 9.8 mmol) and silylated organic product (0.350 g, 0.5 mmol dissolved in water/acetone) was slowly added. After the reactants were mixed, the resulting clear white gel was heated at 100 °C in static conditions for 4 days. The solid obtained was washed thoroughly with water and dried at 100 °C for 3 h. The structure-directing agent was removed by extracting the solid with 0.05 M ethanolic HCl acid solution at 50 °C for 3 h (10 mL of 0.05 M ethanolic HCl for 0.1 g of solid) and then removed by extracting the solid with 0.15 M HCl/EtOH:*n*-heptane (48:52) 90 °C for 12 h (25 mL of 0.15 M HCl/EtOH:*n*-heptane for 0.2 g of solid). Chemical analysis of extracted AZ-2∝PMO gives 3.52 and 0.33% for C and N, respectively.

Adsorption Experiments. Colloidal gold nanoparticles were prepared by treating $HAuCl_4$ with NaOH using tetrakis(hydroxymethyl)phosphonium as stabilizer, following the procedure reported by Maiker and co-workers.[32] Four milliliters of the colloidal gold solution (gold content 10^{-4} mg mL^{-1}) was magnetically stirred at room temperature for 1 h in the presence of the corresponding sample (67 mg). After this time, the suspension was decanted and the supernatant analyzed by UV/Vis spectroscopy.

Acknowledgment. E.P., M.B., and D.D. thank the Universidad Politécnica de Valencia, José Royo Foundation, and Generalitat Valenciana, respectively, for post-graduate scholarships (E.P. and M.B.) and postdoctoral fellowship (D.D.). Financial support by the Spanish Ministry of Science and Technology (MAT03-1763) is gratefully acknowledged.

CM050837Z

(30) Aoyagi, T.; Ueno, A.; Fukushima, M.; Osa, T. *Macromol. Rapid Commun.* **1998**, *19*, 103−105.
(31) Bulacovschi, V.; Hurduc, N.; Scutaru, D.; Simionescu, C. I. *J. Ind. Chem. Soc.* **1994**, *71*, 757−759.
(32) Grunwaldt, J.-D.; Kiener, C.; Wögerbauer, C.; Baiker, A. *J. Catal.* **1999**, *181*, 223−232.